Arch. Mech., **54**, 3, pp. 223–244, Warszawa 2002

The plane single crystal under off-axis uniaxial tension

A. CHENAOUI[(1)], F. SIDOROFF[(2)], M. DARRIEULAT[(3)], A. HIHI[(4)]

[(1)] *L.M.M.H., Faculté des Sciences et Techniques de Tanger, B.P. 416, Tanger, Morocco*

[(2)] *LTDS, UMR, C.N.R.S. 5513, Ecole Centrale de Lyon, B. P. 163, 69131 Ecully Cedex, France*

[(3)] *SMS, M.M.F., U.R.A., C.N.R.S. 1884, Ecole Nationale Supérieure des Mines de Saint Etienne, 158 cours Fauriel, 42023 Saint Etienne Cedex 2, France*

[(4)] *L.M.M., Faculté des Sciences de Rabat, B. P. 1014, Rabat Agdal, Morocco*

THE TENSILE BEHAVIOUR of a rigid-plastic single crystal obeying Schmid's law with isotropic hardening is investigated for an off-axis tensile test in one of its symmetry planes (plane single crystal). Identification of the active slip systems allows the determination of the plastic spin and the resulting evolution of the crystallographic directions. This results in the description of the tensile behaviour-stress and strain response, onset of instability – depending upon the initial orientation of the crystal and the hardening law.

Key words: anisotropic material; crystal plasticity; finite strain; microstructure.

Notations

$\mathbf{F}$	deformation gradient tensor
$\mathbf{P}$	plastic transformation tensor
$\mathbf{R}$	lattice rotation tensor
$\mathbf{L}$	velocity gradient tensor
$\mathbf{D}$	strain-rate tensor
$\mathbf{W}$	rotation rate-tensor
$\bar{\mathbf{D}}$	strain-rate tensor rotated in the crystallographic configuration
$\bar{\mathbf{W}}$	rotation rate-tensor rotated in the crystallographic configuration
$\mathbf{T}$	Cauchy stress tensor
$\bar{\mathbf{T}}$	Cauchy stress tensor rotated in the crystallographic configuration
$\overline{\mathbf{N}}^s$	the s^{th} "pseudo slip" system $\dot{\gamma}^s$ shear strain rate on the "pseudo slip" system(s)

τ^s resolved shear stress on the "pseudo slip" system (s)
τ_c critical resolved shear stress
$\bar{\gamma}$ accumulated slip
τ_0 initial resolved shear stress H, A, n hardening material constants
x_1, x_2, x_3 space coordinates in the laboratory frame
$\bar{x}_1, \bar{x}_2, \bar{x}_3$ space coordinates in the crystallographic frame
θ orientation of the tensile axis
σ tensile stress
ε tensile strain
η transverse strain
ζ shear strain
σ^I stress at the onset of necking
ε^I strain at the onset of necking

1. Introduction

ANISOTROPIC PLASTICITY at large strain is an important problem for many engineering applications and in particular, for deep drawing and metal forming. The anisotropy of the behaviour and its evolution as well as plastic instability are some important features to be described and it is now well understood that the plastic spin is an essential issue to be dealt with.

From a macroscopic point of view, the plastic spin can be either a priori defined from the deformation (kinematic rotating frame [1]) or a posteriori postulated from the evolution equation (plastic spin [2]). It has, for example, recently been shown in [3] that the plastic spin and the initial orientation play a very essential role for instability analysis in an orthotropic material with Hill's quadratic criterion and Loret's plastic spin equation [4].

From a microscopic point of view however, the plastic spin directly follows from the evolution of the crystallographic directions, which in turn results from crystallographic glide along the active systems of each grain. The mechanics of single crystal therefore should play an important part in understanding the plastic spin and its influence upon anisotropy evolution and plastic instability.

The purpose of the present work is to investigate this question in the special case of the off-axis tensile behaviour of a fcc single crystal in one of its symmetry planes (100) or (110). As shown in [5-7], the behaviour of the real 3D crystal can in this case be described through a two-dimensional model: the plane single crystal.

A rigid-plastic model with isotropic hardening will be used and attention will be focussed on the dependence of the tensile behaviour and of the necking limit according to Considère's criterion [8] upon the initial orientation of the crystal and the hardening law.

2. Mechanical framework

2.1. Plane single crystal

A single crystal is a three-dimensional anisotropic material. In general, a two dimensional strain state will result in a three dimensional stress and vice versa. This difficulty is usually skipped by considering some fictitious two-dimensional crystal (double slip model [9-11]).

However, if the 3D single crystal is considered in one of its symmetry plane, then plane stress and plane strain are compatible resulting in a true two-dimensional model: "The plane single crystal" which is defined by the kinematical equations:

$$\mathbf{F} = \mathbf{R}\,\mathbf{P}, \quad \dot{\mathbf{P}}\,\mathbf{P}^{-1} = \sum_{s}^{m} \dot{\gamma}^s \bar{\mathbf{N}}^s, \tag{2.1}$$

where $\mathbf{F}$, $\mathbf{P}$ and $\mathbf{R}$ respectively, denote the deformation gradient, the plastic transformation and the lattice rotation tensors, while $\bar{\mathbf{N}}^s$ is the plane pseudo-slip system, defined in the crystallographic (isoclinic) configuration, which represents the symmetric contribution of two symmetric systems to $\dot{\mathbf{P}}\,\mathbf{P}^{-1}$ ([5-6] and [12]).

The velocity gradient $\mathbf{L}$, strain rate $\mathbf{D} = (\mathbf{L})^S$ and rotation rate $\mathbf{W} = (\mathbf{L})^A$ then result as

$$\mathbf{L} = \dot{\mathbf{F}}\,\mathbf{F}^{-1} = \dot{\mathbf{R}}\,\mathbf{R}^T + \mathbf{R}\,\dot{\mathbf{P}}\,\mathbf{P}^{-1}\,\mathbf{R}^T, \tag{2.2}$$

$$\bar{\mathbf{D}} = \mathbf{R}^T\,\mathbf{D}\,\mathbf{R} = \sum_{s}^{m} \dot{\gamma}^s \left(\bar{\mathbf{N}}^s\right)^S, \tag{2.3}$$

$$\bar{\mathbf{W}} = \mathbf{R}^T\,\mathbf{W}\,\mathbf{R} = \mathbf{R}^T\dot{\mathbf{R}} + \sum_{s}^{m} \dot{\gamma}^s \left(\bar{\mathbf{N}}^s\right)^A, \tag{2.4}$$

where suffices $(\,)^S$ and $(\,)^A$ respectively, denote the symmetric and skew-symmetric part of any tensor, and where a superimposed bar denotes tensors rotated in the crystallographic configuration.

In the following, attention will be focussed on rate-independent plasticity (Schmid's law)

$$\dot{\gamma}^s \geq 0 \quad \text{if} \quad \tau^s = \tau_c\,, \quad \dot{\gamma}^s = 0 \quad \text{if} \quad |\tau^s| < \tau_c, \quad \dot{\gamma}^s \leq 0 \quad \text{if} \quad \tau^s = -\tau_c, \tag{2.5}$$

where τ_c is the critical resolved shear stress, and τ^s is the resolved shear stress defined as

$$\tau^s = \bar{\mathbf{T}}_{ij}\,\bar{\mathbf{N}}^s_{ij}, \quad \bar{\mathbf{T}} = \mathbf{R}^T\mathbf{T}\mathbf{R}, \tag{2.6}$$

with $\mathbf{T}$ being the usual Cauchy stress tensor as observed in the laboratory frame and $\bar{\mathbf{T}}$ the corresponding tensor in the crystallographic configuration.

In this work the uniform isotropic hardening will be assumed with the same τ_c for all systems. The hardening rule is taken as

$$\tau_c = \tau_c(\bar{\gamma}), \tag{2.7}$$

where

$$\dot{\bar{\gamma}} = \sum_s^m |\dot{\gamma}^s| \quad \text{and} \quad \bar{\gamma} = \int_0^T \dot{\bar{\gamma}} dt.$$

Two cases will be considered in the following:
- linear hardening

$$\tau_c = \tau_0(1 + H\,\bar{\gamma}), \tag{2.8}$$

- nonlinear power law hardening

$$\tau_c = \tau_0(1 + A\,(\bar{\gamma})^n), \tag{2.9}$$

where τ_0 is the initial resolved shear and H, A and n are material constants.

In this plane case, the rotation $\mathbf{R}$ and the stress tensor $\mathbf{T}$ are respectively given by

$$R = \begin{bmatrix} \cos(\theta) & \sin(\theta) & 0 \\ -\sin(\theta) & \cos(\theta) & 0 \\ 0 & 0 & 1 \end{bmatrix},$$

$$R^T \dot{R} = \dot{\theta} \begin{bmatrix} 0 & 1 & 0 \\ -1 & 0 & 0 \\ 0 & 0 & 0 \end{bmatrix}, \tag{2.10}$$

$$T = \begin{bmatrix} \sigma_1 & \tau & 0 \\ \tau & \sigma_2 & 0 \\ 0 & 0 & 0 \end{bmatrix},$$

with the following relations:

$$\begin{aligned} \bar{T}_{11} &= \frac{\sigma_1 + \sigma_2}{2} + \frac{\sigma_1 - \sigma_2}{2}\cos(2\theta) - \tau\sin(2\theta), \\ \bar{T}_{22} &= \frac{\sigma_1 + \sigma_2}{2} - \frac{\sigma_1 - \sigma_2}{2}\cos(2\theta) + \tau\sin(2\theta), \\ \bar{T}_{12} &= \frac{\sigma_1 - \sigma_2}{2}\sin(2\theta) + \tau\cos(2\theta). \end{aligned} \tag{2.11}$$

For a fcc single crystal there are 12 systems associated to the planes {111} and directions <110>. This 3D single crystal gives rise to two plane single crystals corresponding to a plane stress and strain state in the {100} and {110} planes, respectively. We shall therefore restrict our attention to these two cases, respectively denoted by Pfcc1 and Pfcc2 (plane fcc) single crystals. The crystallographic frame $(\bar{x}_1, \bar{x}_2, \bar{x}_3)$ is chosen

for Pfcc1 : $\bar{x}_1 = [100]$, $\bar{x}_2 = [010]$, $\bar{x}_3 = [001]$,

for Pfcc2 : $\bar{x}_1 = [001]$, $\bar{x}_2 = [1\bar{1}0]$, $\bar{x}_3 = [110]$.

The corresponding pseudo-slip systems are summarized in Table 1 (Pfcc 2 model) and Table 2 (Pfcc1 model) and the Reader is referred to Refs. [5-7] for further details.

It should be noted that the Pfcc2 single crystal presented here has recently been used by [13-15] for the bicrystal investigation in (110) channel die compression.

Table 1. Pfcc2 single crystal

System (s)	Resolved shear τ^s	Pseudo-slip $\overline{\mathbf{N}}^s$
1	$\tau^1 = \dfrac{\overline{\mathbf{T}}_{12}}{\sqrt{3}}$	$\overline{\mathbf{N}}^1 = \dfrac{1}{2\sqrt{3}}\begin{bmatrix} 0 & 0 \\ 2 & 0 \end{bmatrix}$
2	$\tau^2 = \dfrac{\overline{\mathbf{T}}_{12} - \sqrt{2}\,\overline{\mathbf{T}}_{11}}{2\sqrt{3}}$	$\overline{\mathbf{N}}^2 = \dfrac{1}{2\sqrt{3}}\begin{bmatrix} -\sqrt{2} & 0 \\ 1 & 0 \end{bmatrix}$
3	$\tau^3 = \dfrac{\overline{\mathbf{T}}_{12} + \sqrt{2}\,\overline{\mathbf{T}}_{11}}{2\sqrt{3}}$	$\overline{\mathbf{N}}^3 = \dfrac{1}{2\sqrt{3}}\begin{bmatrix} \sqrt{2} & 0 \\ 1 & 0 \end{bmatrix}$
4	$\tau^4 = \dfrac{\overline{\mathbf{T}}_{12} + \sqrt{2}\,(\overline{\mathbf{T}}_{11} - \overline{\mathbf{T}}_{22})}{2\sqrt{3}}$	$\overline{\mathbf{N}}^4 = \dfrac{1}{2\sqrt{3}}\begin{bmatrix} \sqrt{2} & 2 \\ -1 & -\sqrt{2} \end{bmatrix}$
5	$\tau^5 = \dfrac{\overline{\mathbf{T}}_{12} - \sqrt{2}\,(\overline{\mathbf{T}}_{11} - \overline{\mathbf{T}}_{22})}{2\sqrt{3}}$	$\overline{\mathbf{N}}^5 = \dfrac{1}{2\sqrt{3}}\begin{bmatrix} -\sqrt{2} & 2 \\ -1 & \sqrt{2} \end{bmatrix}$

2.2. Off-axis tensile test

Our attention is focussed here on off-axis tensile test [16], where the Cauchy stress $\mathbf{T}$ and the deformation gradient $\mathbf{F}$ are given, in the laboratory frame (x_1, x_2, x_3), by

$$\mathbf{T} = \begin{bmatrix} \sigma & 0 & 0 \\ 0 & 0 & 0 \\ 0 & 0 & 0 \end{bmatrix}, \quad \mathbf{F} = \begin{bmatrix} e^{\varepsilon} & \zeta e^{\varepsilon} & 0 \\ 0 & e^{\eta} & 0 \\ 0 & 0 & e^{-(\varepsilon+\eta)} \end{bmatrix}. \tag{2.12}$$

Table 2. Pfcc1 single crystal

System (s)	Resolved shear τ^s	Pseudo-slip $\overline{\mathrm{N}}^s$
1	$\tau^1 = \dfrac{\overline{\mathrm{T}}_{11} - \overline{\mathrm{T}}_{22}}{\sqrt{6}}$	$\overline{\mathrm{N}}^1 = \dfrac{1}{\sqrt{6}}\begin{bmatrix} 1 & 1 \\ -1 & -1 \end{bmatrix}$
2	$\tau^2 = \dfrac{\overline{\mathrm{T}}_{11} + \overline{\mathrm{T}}_{12}}{\sqrt{6}}$	$\overline{\mathrm{N}}^2 = \dfrac{1}{\sqrt{6}}\begin{bmatrix} 1 & 1 \\ 0 & 0 \end{bmatrix}$
3	$\tau^3 = \dfrac{\overline{\mathrm{T}}_{22} + \overline{\mathrm{T}}_{12}}{\sqrt{6}}$	$\overline{\mathrm{N}}^3 = \dfrac{1}{\sqrt{6}}\begin{bmatrix} 0 & 0 \\ 1 & 1 \end{bmatrix}$
4	$\tau^4 = \dfrac{\overline{\mathrm{T}}_{11} - \overline{\mathrm{T}}_{12}}{\sqrt{6}}$	$\overline{\mathrm{N}}^4 = \dfrac{1}{\sqrt{6}}\begin{bmatrix} 1 & -1 \\ 0 & 0 \end{bmatrix}$
5	$\tau^5 = \dfrac{\overline{\mathrm{T}}_{12} - \overline{\mathrm{T}}_{22}}{\sqrt{6}}$	$\overline{\mathrm{N}}^5 = \dfrac{1}{\sqrt{6}}\begin{bmatrix} 0 & 0 \\ 1 & -1 \end{bmatrix}$
6	$\tau^6 = \dfrac{\overline{\mathrm{T}}_{11} - \overline{\mathrm{T}}_{22}}{\sqrt{6}}$	$\overline{\mathrm{N}}^6 = \dfrac{1}{\sqrt{6}}\begin{bmatrix} 1 & -1 \\ 1 & -1 \end{bmatrix}$

The strain components ε, η and ζ are given by

$$\frac{h}{h_0} = e^{\varepsilon}, \quad \frac{d}{d_0} = e^{\eta}, \quad \zeta = e^{-(\varepsilon+\eta)}\,\mathrm{tg}(\xi),$$

where (h_0, d_0) and (h, d) respectively, denote the initial and the current length and width of specimen, and where ξ is the rotation of the final section (Fig. 1).

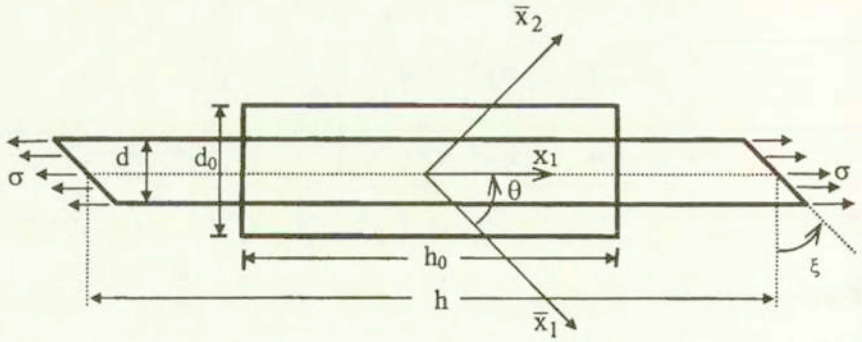

FIG. 1. Off-axis uniaxial tensile test.

The tensile direction x_1 is taken in the crystallographic plane $(\bar{x}_1, \bar{x}_2)$ previously defined.

The lattice angle θ is the angle between the x_1 tensile direction and the fixed lattice orientation $\bar{x}_1$. The strain rate $\mathbf{D}$ and rotation rate $\mathbf{W}$ are obtained from

Eq. (2.12) as

$$D_{11} = \dot{\varepsilon} \ , \ D_{22} = \dot{\eta} \ , \ D_{12} = W_{12} = \frac{\dot{\zeta}}{2} e^{\varepsilon - \eta}, \tag{2.13}$$

or in terms of the rotated tensor $\bar{\mathbf{D}}$ introduced in Eq. (2.3)

$$\begin{aligned} \dot{\varepsilon} &= \frac{\bar{D}_{11} + \bar{D}_{22}}{2} + \frac{\bar{D}_{11} - \bar{D}_{22}}{2} \cos(2\theta) + \bar{D}_{12} \sin(2\theta), \\ \dot{\eta} &= \frac{\bar{D}_{11} + \bar{D}_{22}}{2} - \frac{\bar{D}_{11} - \bar{D}_{22}}{2} \cos(2\theta) - \bar{D}_{12} \sin(2\theta), \\ \dot{\zeta} &= 2e^{(\eta - \varepsilon)} \left\{ -\frac{\bar{D}_{11} - \bar{D}_{22}}{2} \sin(2\theta) + \bar{D}_{12} \cos(2\theta) \right\}, \end{aligned} \tag{2.14}$$

where $\bar{D}_{ij}$ are given from $\dot{\gamma}^s$ by Eq. (2.3) and Table 1 (resp. table 2) for Pfcc2 (resp. Pfcc1) single crystal.

Similarly, by combining Eqs. (2.4), (2.6), (2.10) and (2.13), the lattice spin equation and the rotated stress tensor $\bar{\mathbf{T}}$ can be expressed as

$$W_{12} = \dot{\theta} + \frac{1}{2} \sum_{s}^{m} \dot{\gamma}^s \left\{ \bar{N}^s_{12} - \bar{N}^s_{21} \right\}, \tag{2.15}$$

$$\bar{T}_{11} = \frac{\sigma}{2}(1 + \cos(2\theta)), \quad \bar{T}_{22} = \frac{\sigma}{2}(1 - \cos(2\theta)), \quad \bar{T}_{12} = \frac{\sigma}{2} \sin(2\theta). \tag{2.16}$$

3. The Pfcc 2 single crystal

3.1. System activity

According to Eq. (2.16) and Table 1, the resolved shear stresses τ^s are given by

$$\tau^s = f^s(\theta) \ \sigma, \tag{3.1}$$

where the functions $f^s(\theta)$ are respectively defined by

$$\begin{aligned} f^1(\theta) &= \frac{1}{2\sqrt{3}} \left\{ \sin(2\theta) \right\}, \\ f^2(\theta) &= \frac{1}{4\sqrt{3}} \left\{ -\sqrt{2} + \sin(2\theta) - \sqrt{2} \cos(2\theta) \right\}, \\ f^3(\theta) &= \frac{1}{4\sqrt{3}} \left\{ \sqrt{2} + \sin(2\theta) + \sqrt{2} \cos(2\theta) \right\}, \\ f^4(\theta) &= \frac{1}{4\sqrt{3}} \left\{ \sin(2\theta) + 2\sqrt{2} \cos(2\theta) \right\}, \\ f^5(\theta) &= \frac{1}{4\sqrt{3}} \left\{ \sin(2\theta) - 2\sqrt{2} \cos(2\theta) \right\}. \end{aligned} \tag{3.2}$$

For a given θ, there will usually be one active system corresponding to the maximum absolute value of the five quantities f^s defined in relation (3.2). The corresponding system activity is described as a function of θ in Table 3 with $\mathrm{tg}(2\theta_p) = 2\sqrt{2}$. The tensile stress now follows as a function of θ by

$$\sigma = \frac{\tau_c}{|\, f^s(\theta)\,|}. \tag{3.3}$$

Table 3. System activity for the Pfcc2 single crystal

θ	Active system	Activity conditions	Slip rates
0			
	3^+	$\tau^3 = \tau_c$ and $\dot{\tau}^3 = \dot{\tau}_c$	$\dot{\gamma}^3 \geq 0$
$\pi/2 - \theta_p$			
	5^+	$\tau^5 = \tau_c$ and $\dot{\tau}^5 = \dot{\tau}_c$	$\dot{\gamma}^5 \geq 0$
$\pi/2$			
	4^-	$\tau^4 = -\tau_c$ and $\dot{\tau}^4 = -\dot{\tau}_c$	$\dot{\gamma}^4 \leq 0$
$\pi/2 + \theta_p$			
	2^-	$\tau^2 = -\tau_c$ and $\dot{\tau}^2 = -\dot{\tau}_c$	$\dot{\gamma}^2 \leq 0$
π			

The corresponding curve $\dfrac{\sigma}{\tau_c}$ is represented in Fig. 2.

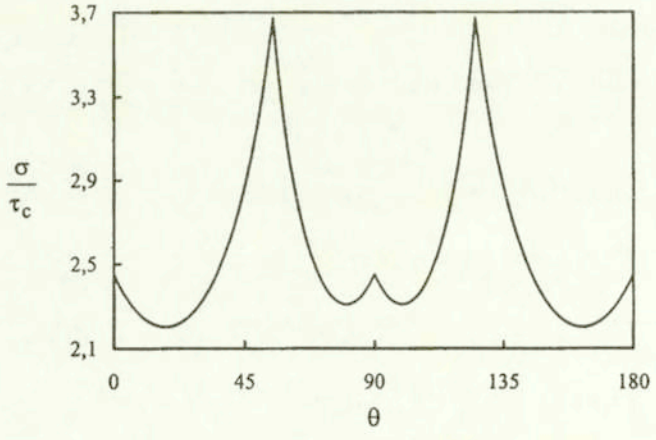

FIG. 2. The Pfcc 2 versus $\dfrac{d\theta}{d\varepsilon}$ versus the crystal orientation θ.

3.2. Lattice rotation

Once the active system is known, the kinematical analysis directly proceeds from the relations (2.3) and (2.15). Since the system (1) is never active, these equations are reduced to

$$\bar{D}_{11} = \frac{1}{\sqrt{6}}\left\{\dot{\gamma}^3 + \dot{\gamma}^4 - \dot{\gamma}^5 - \dot{\gamma}^2\right\},$$

$$\bar{D}_{22} = \frac{1}{\sqrt{6}}\left\{\dot{\gamma}^5 - \dot{\gamma}^4\right\}, \tag{3.4}$$

$$\bar{D}_{12} = \frac{1}{4\sqrt{3}}\left\{\dot{\gamma}^2 + \dot{\gamma}^3 + \dot{\gamma}^4 + \dot{\gamma}^5\right\},$$

$$W_{12} = \dot{\theta} - \frac{1}{4\sqrt{3}}\left\{3\dot{\gamma}^4 + 3\dot{\gamma}^5 - \dot{\gamma}^2 - \dot{\gamma}^3\right\}. \tag{3.5}$$

For instance, if the active system is the system (3), the Eq. (3.4) becomes

$$\bar{D}_{11} = \frac{1}{\sqrt{6}}\dot{\gamma}^3, \quad \bar{D}_{22} = 0, \quad \bar{D}_{12} = \frac{1}{4\sqrt{3}}\dot{\gamma}^3, \tag{3.6}$$

which give from Eq. (2.14)

$$\dot{\gamma}^3 = \frac{\dot{\varepsilon}}{f^3(\theta)}, \tag{3.7}$$

with the same function $f^3(\theta)$ as in Eq. $(3.2)_3$.

Using Eqs. (2.13), (2.14), (3.5) and (3.6), the component W_{12} can be written as

$$W_{12} = \frac{\dot{\zeta}}{2}e^{(\varepsilon-\eta)} = \frac{\cos(2\theta) - \sqrt{2}\sin(2\theta)}{4\sqrt{3}\,f^3(\theta)}\dot{\varepsilon}. \tag{3.8}$$

Combining Eqs. (3.7) and (3.8), the evolution Eq. (3.5) gives $\frac{\dot{\theta}}{\dot{\varepsilon}} = \frac{d\theta}{d\varepsilon}$ as

$$\frac{d\theta}{d\varepsilon} = \frac{g^3(\theta)}{f^3(\theta)}, \tag{3.9}$$

where

$$g^3(\theta) = \frac{1}{4\sqrt{3}}\left\{1 - \sqrt{2}\sin(2\theta) + \cos(2\theta)\right\}. \tag{3.10}$$

The other cases are analyzed in a similar way. More generally, we obtain for each active system (s)

$$\dot{\gamma}^s = \frac{\dot{\varepsilon}}{f^s(\theta)}, \tag{3.11}$$

$$\frac{d\theta}{d\varepsilon} = \frac{g^s(\theta)}{f^s(\theta)}, \tag{3.12}$$

where the functions $f^s(\theta)$ are defined in Eqs. (3.2) and $g^s(\theta)$ are respectively, defined by

$$\begin{aligned}
g^2(\theta) &= \frac{1}{4\sqrt{3}}\left\{1+\sqrt{2}\sin(2\theta)+\cos(2\theta)\right\}, && 0 \le \theta \le \frac{\pi}{2}-\theta_p,\\
g^3(\theta) &= \frac{1}{4\sqrt{3}}\left\{1-\sqrt{2}\sin(2\theta)+\cos(2\theta)\right\}, && \frac{\pi}{2}-\theta_p \le \theta \le \frac{\pi}{2},\\
g^4(\theta) &= \frac{1}{4\sqrt{3}}\left\{-3-2\sqrt{2}\sin(2\theta)+\cos(2\theta)\right\}, && \frac{\pi}{2} \le \theta \le \frac{\pi}{2}+\theta_p,\\
g^5(\theta) &= \frac{1}{4\sqrt{3}}\left\{2\sqrt{2}\sin(2\theta)+\cos(2\theta)-3\right\}, && \frac{\pi}{2}+\theta_p \le \theta \le \pi.
\end{aligned} \tag{3.13}$$

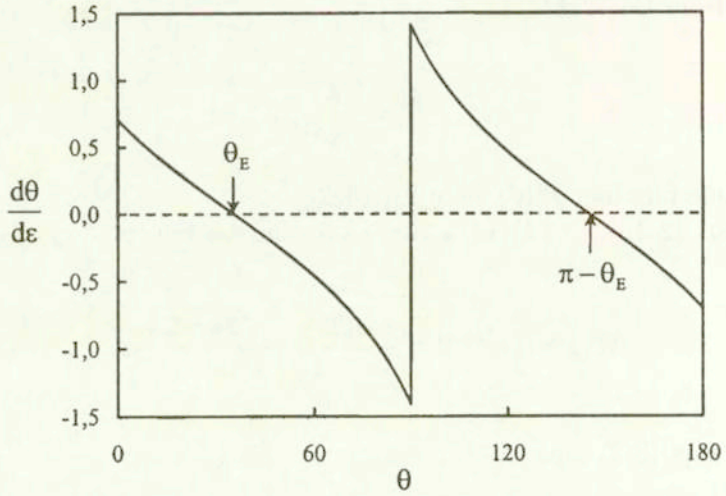

FIG. 3. The Pfcc 2 plastic spin $\frac{d\theta}{d\varepsilon}$ versus the crystal orientation θ.

The function $\frac{d\theta}{d\varepsilon}$ is represented in Fig. 3. The lattice rotation evolution, from its initial value θ_0, directly follows from this curve. For instance, if $0 \le \theta_0$

$\leq \theta_E\left(\mathrm{tg}(\theta_E) = \dfrac{1}{\sqrt{2}}\right)$, $\dfrac{d\theta}{d\varepsilon}$ is positive so that θ increases and tends to the stable orientation θ_E, while if $\theta_E \leq \theta_0 \leq \pi/2$, θ decreases toward the same stable orientation. Similar results are obtained for $\pi/2 \leq \theta_0 \leq \pi$. This evolution is represented in Fig. 4.

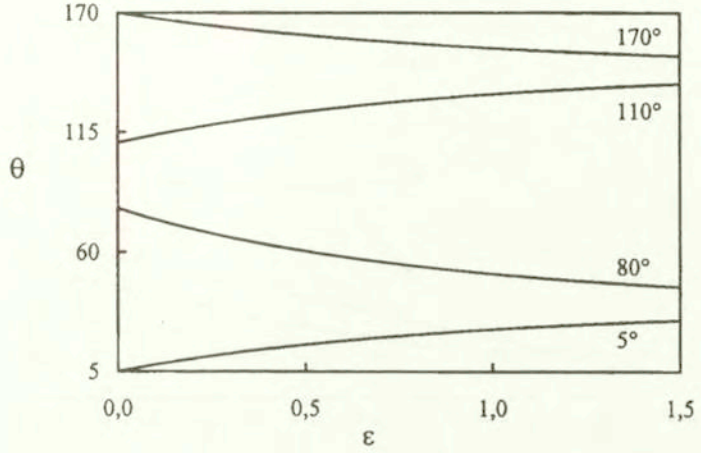

FIG. 4. The Pfcc 2 lattice spin versus the strain ε, for various values of initial orientation θ_0.

3.3. Stress and strain response

The stress response $\sigma(\varepsilon)$ directly follows as

$$\sigma(\varepsilon) = \frac{\tau_c(\bar{\gamma})}{|\, f^s(\theta)\,|}, \tag{3.14}$$

where θ and $\bar{\gamma}$ are obtained, as a function of ε, through the integration of the expression (3.11) and (3.12) of $\dfrac{d\gamma}{d\varepsilon}$ and $\dfrac{d\theta}{d\varepsilon}$.

This response is illustrated in Figs. 5a-b (linear hardening) and Figs. 6a-b (power law), for various values of θ_0. It can be seen that, depending on the crystal orientation and on the hardening rule, the tensile response σ may be an increasing or decreasing function of ε (a negative or a positive hardening). Negative hardening however will decrease when the mechanical hardening increases. This is illustrated in Fig. 7 which for linear hardening shows the angular region corresponding to tensile negative hardening as a function of the hardening parameter H. In particular, negative hardening disappears for $H \simeq 0.4$ which is a rather high value.

Similarly, for the strain, the corresponding differential system, which by integration gives η and ζ in terms of ε, is easily obtained from Eqs. (2.14), (3.4), (3.11) and (3.12).

The corresponding evolution, which in fact does not depend on the hardening, is plotted in Figs. 8a-b for different values of θ_0. These results illustrate clearly the effect of rotation on the single crystal behaviour.

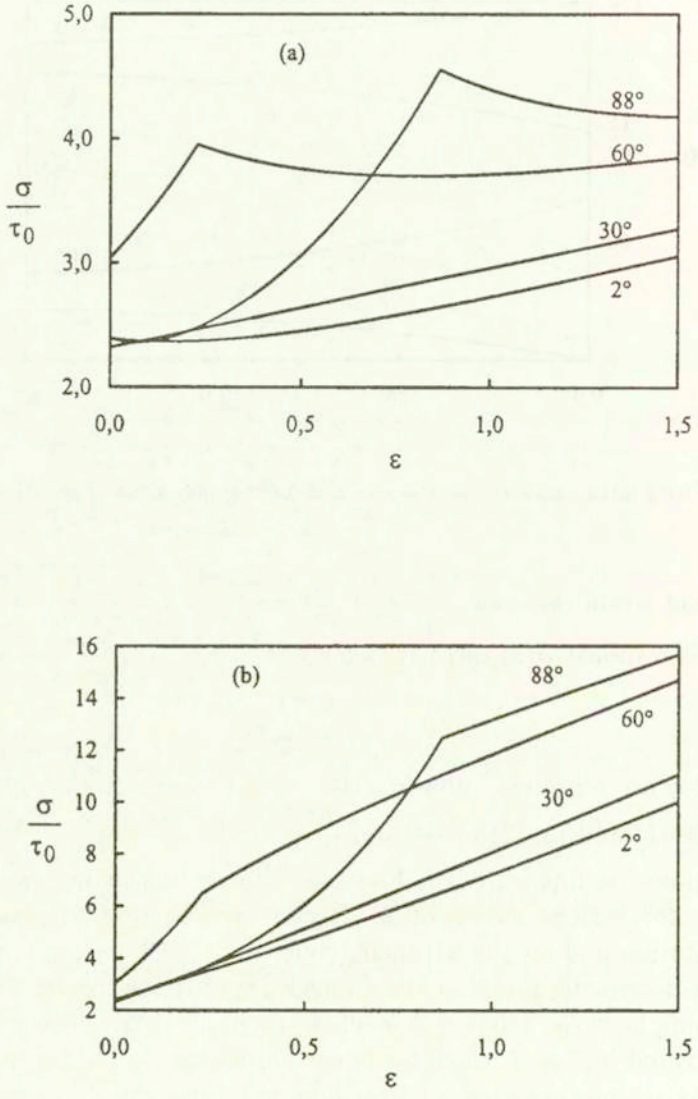

FIG. 5. The Pfcc 2 tensile response σ versus the strain ε, for various values of initial orientation θ_0 and with linear hardening. (a) when $H = 0.1$ (b) when $H = 1$.

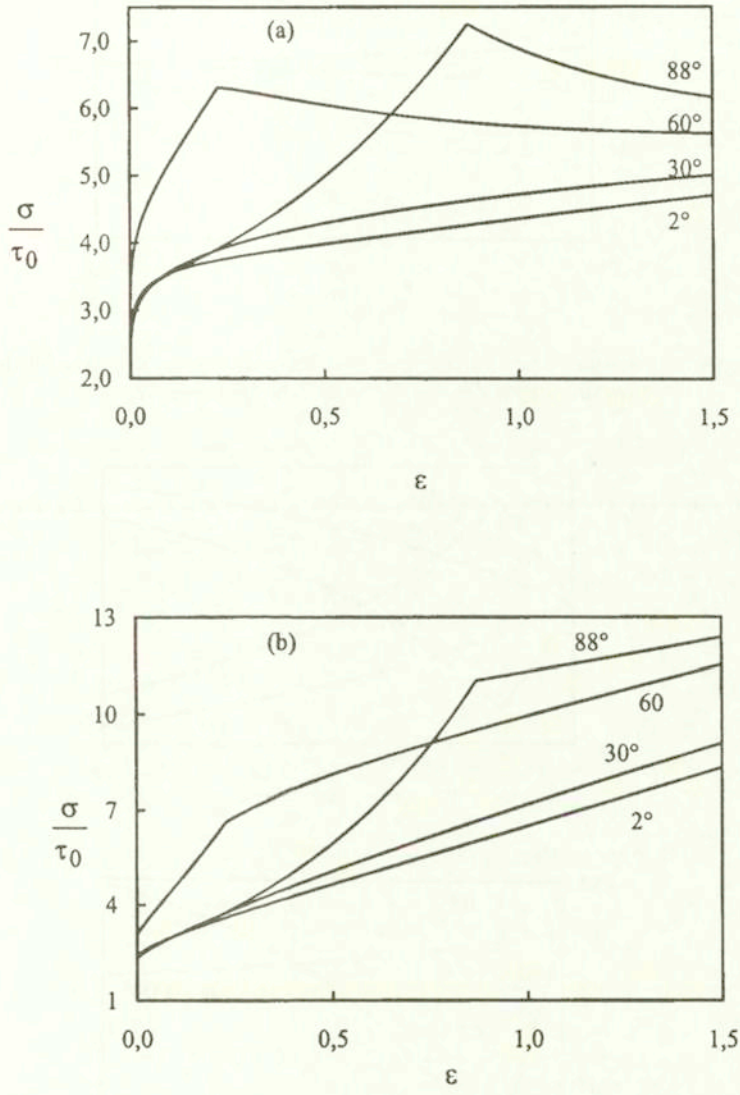

FIG. 6. The Pfcc 2 tensile response σ versus the strain ε, for various values of initial orientation θ_0 and with power law hardening. (a) when $A = 1$ and $n = 0.2$, (b) when $A = 1$ and $n = 0.8$

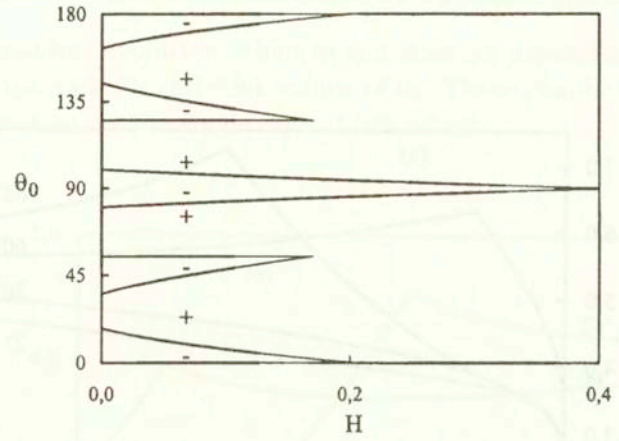

FIG. 7. The Pfcc 2 angular region (H, θ_0) corresponding to tensile negative hardening as a function of hardening parameter H for linear law.

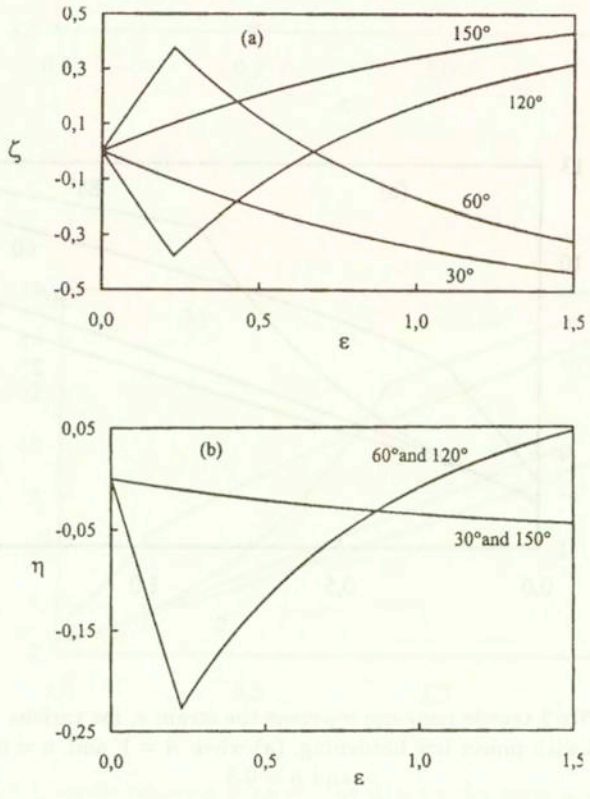

FIG. 8. The Pfcc 2 strain response for various values of initial orientation; (a) the shear ζ versus the strain ε, (b) the transverse strain η versus the strain ε.

4. Plastic instability

4.1. Considère's analysis

We are now interested in the necking instability which may occur during a tensile test. Considère's necking criterion is used [8], which associates necking to the maximum of the tensile force $P = S\sigma = S_0\sigma e^{-\varepsilon}$ (plastic incompressibility), leading to the following criterion:

$$\frac{1}{\sigma}\frac{d\sigma}{d\varepsilon} = 1. \tag{4.1}$$

In this relation σ is given by Eq. (3.14), while $\dfrac{d\sigma}{d\varepsilon}$ is calculated, for each active system (s), from the activation condition (2.5)

$$\dot{\sigma}^s = \operatorname{sgn}(f^s)\dot{\tau}_c, \tag{4.2}$$

where sgn(x) is the sign of the scalar quantity x.

Using Eq. (3.1), this gives

$$\sigma\frac{df^s}{d\theta}\frac{g^s}{f^s} + f^s\frac{d\sigma}{d\varepsilon} = \operatorname{sgn}(f^s)\frac{d\tau_c}{d\varepsilon},$$

providing $\dfrac{d\sigma}{d\varepsilon}$ as:

- for linear hardening (Eq. (2.8))

$$\frac{d\sigma}{d\varepsilon} = \frac{H\tau_0 - \Psi^s}{(f^s)^2}, \tag{4.3}$$

- for nonlinear hardening (Eq. (2.9))

$$\frac{d\sigma}{d\varepsilon} = \frac{nA\tau_0\ (\bar{\gamma})^{n-1} - \Psi^s}{(f^s)^2}, \tag{4.4}$$

where the function $\Psi^s(\theta, \sigma)$ is defined by

$$\Psi^s(\theta, \sigma) = g^s\frac{df^s}{d\theta}\sigma.$$

For a given tensile test the stress σ^I and strain ε^I, corresponding to the onset of necking, are then easily deduced from the criterion introduced in Eq. (4.1).

4.2. Applications

The values of σ^I and ε^I, as a function of the initial orientation θ_0 and for different cases of hardening, are represented in Figs. 9a-b and 10a-b.

This illustrates the combined effect of hardening and orientation on necking. It should be noted that in agreement with Fig. 7, necking can happen from the very beginning ($\varepsilon^I = 0$). The corresponding region in the (θ_0, H)-plane (for linear hardening) is represented in Fig. 11.

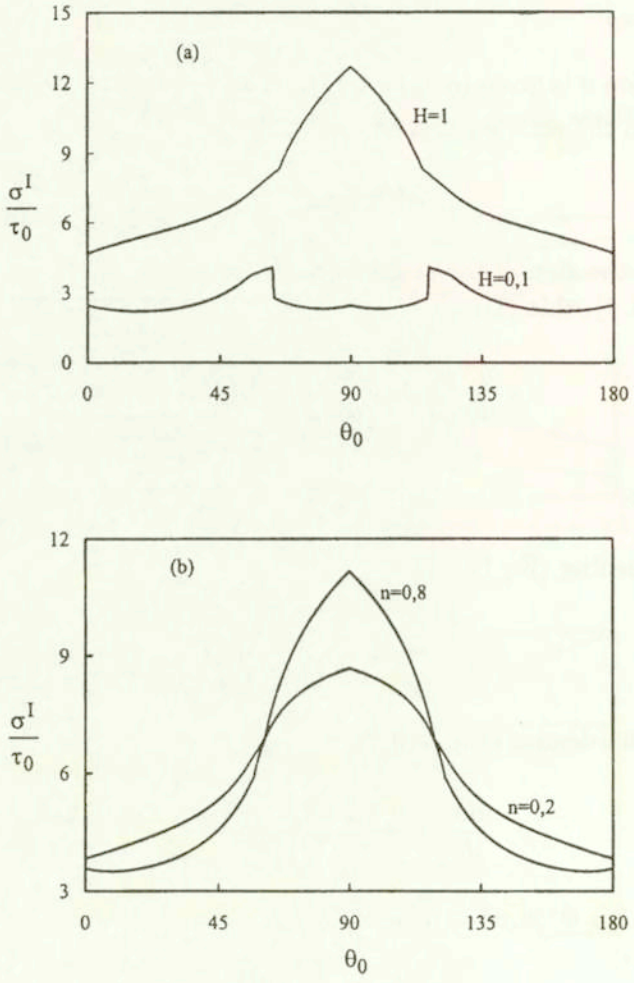

FIG. 9. The Pfcc 2 tensile stress σ^I at the onset of necking versus the initial orientation θ_0 (a) linear hardening, (b) power law hardening when $A = 1$.

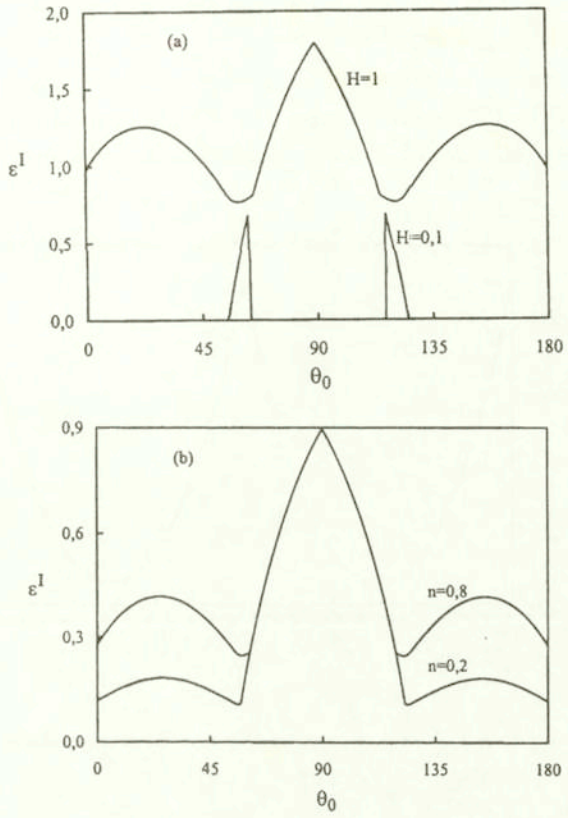

FIG. 10. The Pfcc 2 tensile strain ε^I at the onset of necking versus the initial orientation θ_0; (a) linear hardening, (b) power law hardening when $A = 1$.

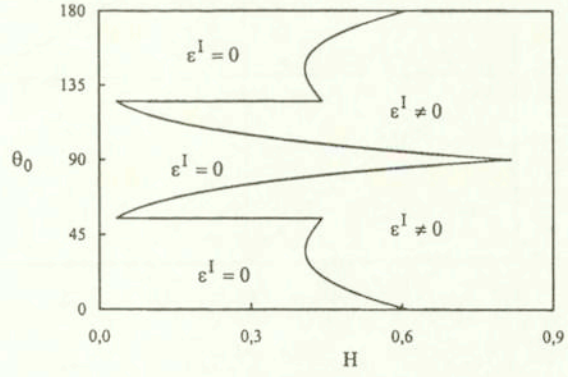

FIG. 11. The Pfcc 2 initial orientation as function of linear hardening parameter H corresponding to $\varepsilon^I = 0$.

5. The Pfcc 1 behaviour

Similar analysis can be performed in the Pfcc1 case and the corresponding results (Figs. 12-16 and Tabl. 4) are presented below without further details.

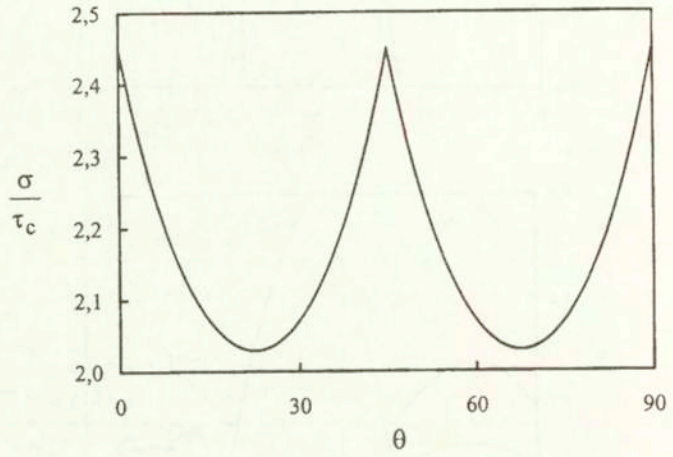

FIG. 12. The Pfcc 1 $\frac{\sigma}{\tau_c}$ versus the crystal orientation θ.

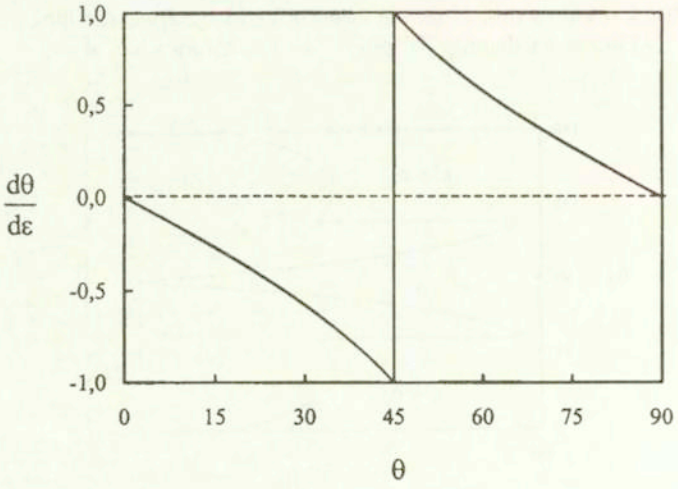

FIG. 13. The Pfcc 1 plastic spin $\frac{d\theta}{d\varepsilon}$ versus the crystal orientation θ.

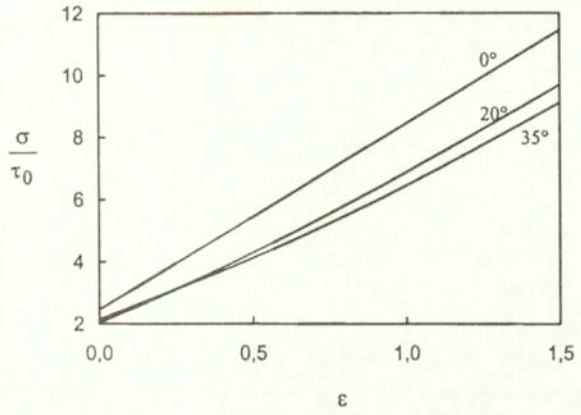

FIG. 14. The Pfcc 1 tensile response σ versus the strain ε, for various values of initial orientation θ_0. Linear hardening when $H = 1$.

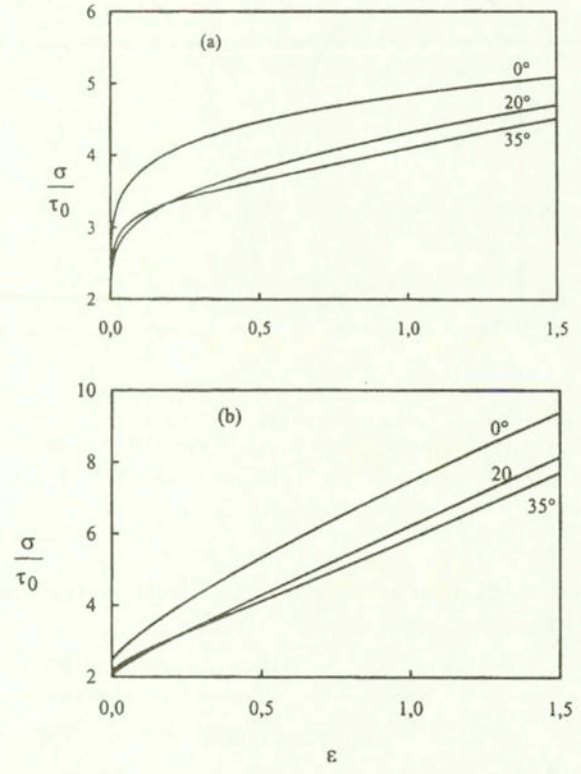

FIG. 15. The Pfcc 1 tensile response σ versus the strain ε, for various values of initial orientation θ_0. Power law hardening with $A = 1$: (a) when $n = 0.2$; (b) when $n = 0.8$.

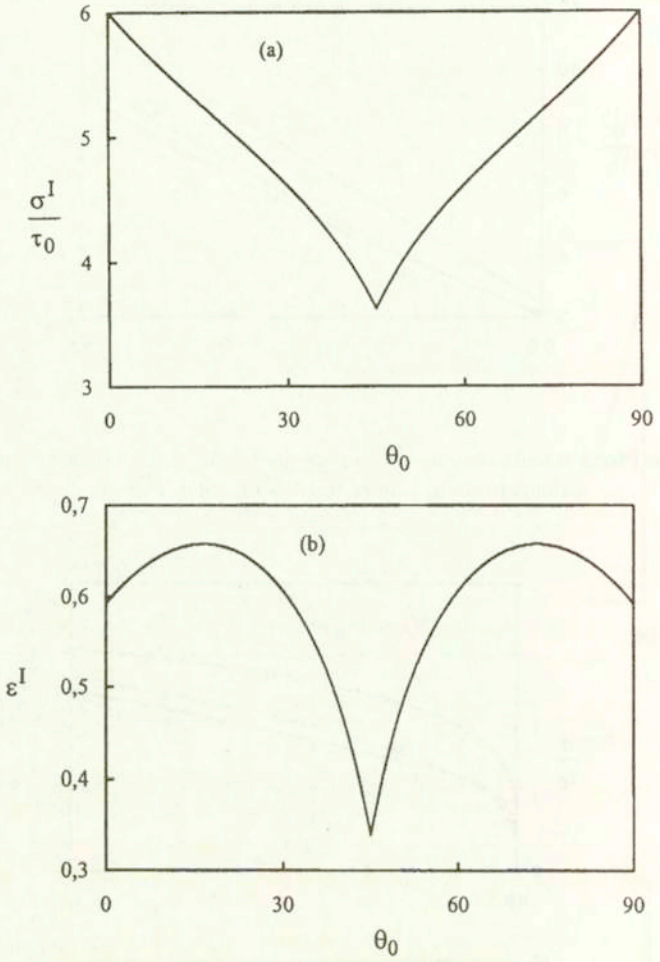

FIG. 16. The Pfcc 1 tensile stress $\sigma^I(a)$ and strain ε^I (b) at the onset of necking versus the initial orientation θ_0, for linear hardening with $H = 1$.

Table 4. System activity for the Pfcc1 single crystal

θ	Active system	Activity conditions	Slip rates
0			
	2^+	$\tau^2 = \tau_c$ and $\dot{\tau}^2 = \dot{\tau}_c$	$\dot{\alpha}^2 \geq 0$
$\pi/4$			
	3^+	$\tau^3 = \tau_c$ and $\dot{\tau}^3 = \dot{\tau}_c$	$\dot{\alpha}^3 \geq 0$
$\pi/2$			

6. Conclusions

A f.c.c. single crystal undergoing stress in one of its symmetry planes {110} or {100} retains this element of symmetry throughout the deformation. Taking advantage of the consequent simplifications, a fully analytical investigation of the plastic behaviour is possible in the case of large strain deformations.

In the present paper, the case of the off-axis uniaxial tension of a rigid plastic crystal is presented. Double slip is activated from the onset on symmetric slip systems, leading to a case of "plane deformation" that can actually be observed in real crystals. Strain hardening is taken as isotropic, but with various hypotheses. The rotation of the crystal with respect to the tensile axis is calculated, and stability is put in evidence when the tension is performed along the $< 1\bar{1}2 >$ direction (plane of symmetry {110}) or the $< 001 >$ direction (plane of symmetry {100}) . The possibility of softening is put in evidence for specific ranges of the initial orientation. The dependence of the threshold of strain localisation on a combination of crystal rotation and strain hardening effects is shown in the simple case of Considère's criterion.

This study completes previous investigations on the simple shear and the torsion in similar symmetry conditions, aiming at a full understanding of the two-dimensional behaviour of crystals.

Acknowledgements

This work was supported in part by the Morocco National Center of Coordination and Planning of Scientific and Technique Research (PARS Program SPI N ° 101) and one of the authors (A.C.) wants to express his gratitude to Region Rhone-Alpes for generous financial support of his stay at the Ecole des Mines de Saint Etienne.

References

1. A. DOGUI and F. SIDOROFF, *Rhéologie anisotrope en grandes déformations,* [in:] Proc. Conf. on Rhéologie des Materiaux Anisotropes C. HUET, D. BOURGON and S. RICHEMOND)[Eds.], CEPADUES, Toulouse, 69–78, 1986.
2. Y. F. DAFALIAS, *The spin plastic,* J. Appl. Mech., ASME **52**, 865–871, 1985.
3. H. LEE, IM S. and S. N. ATLURI, *Strain localization in an orthotropic material with plastic spin,* Int. J. of Plasticity, **11**, 4, 423–450, 1995.
4. B. LORET and Y. F. DAFALIAS, *The effect of anisotropy and plastic spin on fold deformations,* J. Mech. Phys. Solids, **40** 417, 1992.
5. J. BOUKADIA and F. SIDOROFF, *Simple shear and torsion of a perfectly plastic single crystal in finite transformation,* Arch. Mech. **40**, 497-513, 1988.

6. J. BOUKADIA, A. CHENAOUI and F. SIDOROFF, *Simple shear in fcc single crystals at large deformations,* in Proc. Int. Sem. MECAMAT'91 Faintainebleau /France/ on Large Plastic Deformation C. TEODOSIU, J. L. RAPHANEL and F. SIDOROFF. Rotterdam Balkema, 109-116, 1993.

7. A. CHENAOUI, F. SIDOROFF and A. HIHI, *The texture evolution of planar polycrystal,* J. Mech. Phys. Solids, **48**, 2559-2584, 2000.

8. A. CONSIDÈRE, *Mémoire sur l'emploi du fer et de l'acier dans les constructions,* Annales des Ponts et Chaussées, **9**, 574, 1858.

9. R. J. ASARO, *Geometrical effects in the inhomogeneous deformation of ductile single crystals,* Acta Metall. **27**, 445-453, 1979.

10. K S. HAVNER, *The kinematics of double slip with application to cubic crystals in the compression test,* J. Mech. Phys. Solids, **27**, 415-429, 1979.

11. A. H. SHALABY and K. S. HAVNER, *A general kinematical analysis of double slip,* J. Mech. Phys. Solids, **26**, 79-92, 1978.

12. A. CHENAOUI, *Contribution à l'étude du comportement du monocristal en grandes déformations plastique,* Thesis, Ecole Centrale de Lyon, N° 92-13, 1992.

13. K. S. HAVNER, S.-C. WU and S. FUH, *On symmetric bicrystals at the yield point in (110) channel die compression,* J. Mech. Phys. Solids, **42**, 361-379, 1994.

14. K. S. HAVNER, *On velocity discontinuities in elastoplastic bicrystals in channel die compression,* Int. J. of Plasticity, **14**, 61-74, 1998.

15. P. YU and K. S. HAVNER, *Numerical studies of nonuniform deformation, stress state evolution, and subgrain formation in bicrystals in (110) channel die compression,* J. Mech. Phys. Solids, **49**, 173-208, 2001.

16. A. DOGUI, Cinématique bidimensionnelle en grandes déformations - Application à la traction hors axes et la torsion, J. Méca. Th. et Appl., **7**, 1, 43-64, 1988.

Received January 03, 2002.